Quaternary Science Reviews 313 (2023) 108200

Contents lists available at ScienceDirect

Quaternary Science Reviews

journal homepage: www.elsevier.com/locate/quascirev

Neanderthal footprints in the "Matalascañas trampled surface" (SW Spain): new OSL dating and Mousterian lithic industry

Carlos Neto de Carvalho [a, b], Fernando Muñiz [c], Luis M. Cáceres [d, *], Joaquín Rodríguez-Vidal [d], Alicia Medialdea [e], Miren del Val [e], Pedro Proença Cunha [f], Jose María García [g], Francisco Giles-Guzmán [h], José S. Carrión [i], Zain Belaústegui [j, k], Antonio Toscano [d], Paula Gómez [d], José María Galán [l], João Belo [m], Mario Cachão [b, n], Francisco Ruiz [d], Samuel Ramirez-Cruzado [d], Geraldine Finlayson [h, o], Stewart Finlayson [h], Clive Finlayson [h, o]

[a] Naturtejo UNESCO Global Geopark, Geology Office of the Municipality of Idanha-a Nova, Idanha-a-Nova, Portugal
[b] Instituto D. Luiz, University of Lisbon, Lisbon, Portugal
[c] Department of Crystallography, Mineralogy and Agricultural Chemistry, Faculty of Chemistry, University of Seville, C/Prof. García González, s/n, 41012, Seville, Spain
[d] Departament of Earth Sciences, Faculty of Experimental Sciences, El Carmen Campus, University of Huelva, 21071, Huelva, Spain
[e] National Research Centre on Human Evolution (CENIEH), Paseo de Atapuerca 3, 09002, Burgos, Spain
[f] Department of Earth Sciences, MARE-Marine and Environmental Sciences Centre, University of Coimbra, Coimbra, Portugal
[g] Provincial Archaeological Museum, Avda. Alameda Sundheim, 13, 21003, Huelva, Spain
[h] The Gibraltar National Museum, Gibraltar, UK
[i] Department of Plant Biology (Botany Area), Faculty of Biology, University of Murcia, Campus de Espinardo, 30100 Murcia, Spain
[j] Departament de Dinàmica de la Terra i de L'Oceà, Facultat de Ciències de la Terra, Spain
[k] Institut de Recerca de la Biodiversitat, Universitat de Barcelona, Barcelona, Spain
[l] Administrative Center of El Acebuche, Doñana National Park, Matalascañas, Huelva, Spain
[m] Geosciences Center, University of Coimbra, FlyGIS-UAV Surveys, Coimbra, Portugal
[n] Department of Geology, Faculty of Sciences, University of Lisbon, 1749-016 Lisbon, Portugal
[o] Department of Life Sciences, Liverpool John Moores University, Liverpool, UK

ARTICLE INFO

Article history:
Received 29 April 2023
Received in revised form
18 June 2023
Accepted 22 June 2023
Available online 6 July 2023

Handling Editor: Dr Donatella Magri

Keywords:
Hominin footprints
OSL dating
Lithic industry
Mousterian
Neanderthals

ABSTRACT

In the Huelva Coast of SW Spain erosion by recent marine storms revealed the presence of a paleosol where an extensive tracksite known as "Matalascañas Trampled Surface" (MTS) has been documented. The MTS includes tracks and trackways of large species of mammals, along with bird trace fossils, invertebrate burrows and root traces. Within this record, the presence of several hominin footprints and trackways stands out. Despite previous uncertainties about the producer of these footprints, new OSL age of 151 ± 11 ka secures their attribution to Neanderthals, the only hominins known to have been present in the Iberian Peninsula during the MIS6-5 transition. Moreover, typical Mousterian lithic industry with Levallois knapping was found associated with the ichnological record. This lithic industry is characterized by the selection of raw materials from outcrops in a short-distance range to the tracksite. The general characteristics of the lithics are derived both from the nature of the raw material and from the nature of the site itself, which cannot be seen as a settlement, but rather as a place of passage for fauna, including Neanderthals, where a few human individuals performed short-term activities, such as food procurement and/or meat processing.

1. Introduction

Spring storms of 2020 substantially eroded the base of the El Asperillo Cliff (Matalascañas, Huelva, SW Spain) (Fig. 1A), revealing an extensive surface with abundant animal tracks and trackways.

* Corresponding author.
E-mail address: mcaceres@uhu.es (L.M. Cáceres).

https://doi.org/10.1016/j.quascirev.2023.108200

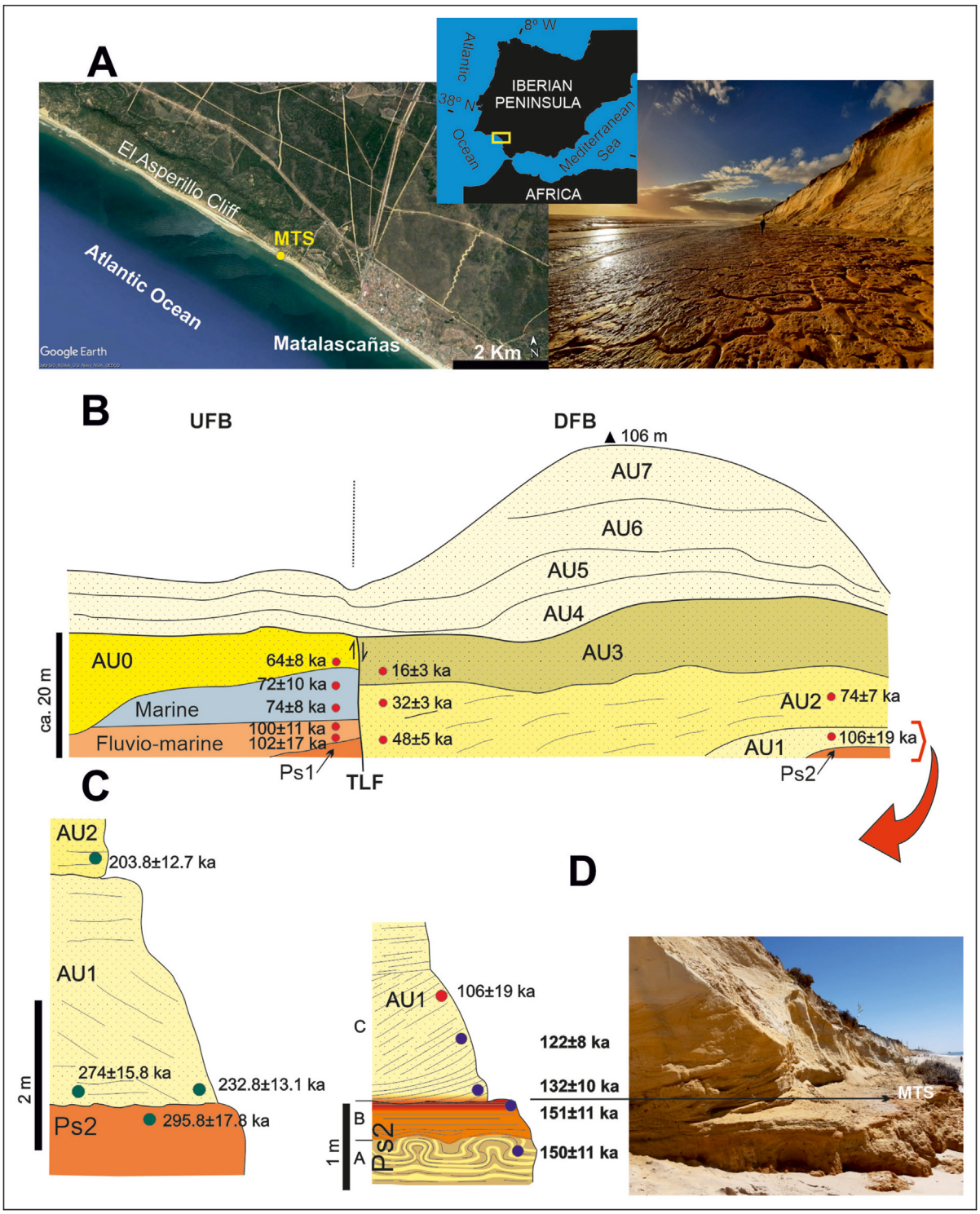

Fig. 1. Location of the MTS within the sedimentary succession of the El Asperillo Cliff and previous and new geochronological data, for comparisons. (A) Location of the El Asperillo Cliff, image adapted from GoogleEarth©. (B) Schematic cross-section along the El Asperillo Cliff, showing the distribution of sedimentary units and palaeosols. Torre del Loro Fault (TLF); Upthrown Fault Block (UFB) and Downthrown Fault Blocks (DFB). Unit nomenclature follows Zazo et al. (2005) (red point), MTS corresponding to the top of Ps2. Note the strong vertical exaggeration (modified from Zazo et al., 2005; Roquero et al., 2013). Geochronological data are those published by Zazo et al. (2005) using OSL, with 1 sigma errors, for comparisons. (C) Schematic stratigraphic column of the cliff for units Ps2 to AU2 in the Matalascañas tracksite and OSL dating, according to Mayoral et al. (2022) (green point). D) New stratigraphic column for units Ps2 to AU1 and OSL dating results obtained in this work (blue point).

The surface remained uncovered for a short time interval and was subjected to intensive studies, being known as "Matalascañas Trampled Surface" (MTS) (Neto de Carvalho et al., 2020a). It was possible to describe in the MTS various trackways and traces corresponding to different types of large mammals (straight-tusked elephant *Palaeoloxodon antiquus*, wild boar *Sus scrofa*, red deer *Cervus elaphus*, aurochs *Bos primigenius*, wolf *Canis lupus*) and birds (Anseriformes: geese, ducks and allies) (Neto de Carvalho et al.,

2020a, 2020b, 2021, 2022). In this same trampled surface, it was possible to document hominin isolated footprints (Mayoral et al., 2021) and two-to-three footprint trackways (Neto de Carvalho et al., 2021). Since de discovery of the MTS, regular studies have been detailing the paleoecology of this coastal interdune, seasonal lacustrine system, as a congregation site where different mammals, including hominins, and birds converged presumably for water and food resources, and possibly also for reproduction.

Initially, MTS was attributed to a Late Pleistocene age (MIS 5) >106 ± 19 ka based on the previous Optically Stimulated Luminescence (OSL) age obtained for the unit above the MTS (Zazo et al., 2005) (Fig. 1B). The tracksite level was recently dated to ~296 ka (Fig. 1C) by Mayoral et al. (2022), opening a new geochronological scenario, compared with previous studies, and raising questions regarding the age of the MTS and consequently, the possible species of hominin that could have produced the footprints.

The aims of this work are: (1) to reinforce the importance of obtaining a precise and reliable geochronological framework for the MTS and its immediate units within the succession, with new OSL dates and a lithic industry consistent with Mousterian technological modes; (2) to compare with the ages available in the area by Zazo et al. (2005) and Mayoral et al. (2022); and (3) to establish the producer of hominin footprints and lithics described in MTS, as their role in the local ecosystem.

2. OSL dates: luminescence dating

2.1. Methodology

To establish a high resolution geochronological frame for the MTS, a total of four sediment samples were collected for OSL dating (Fig. 1D): HU-20-01 from the layer immediately below (layer A), HU-21-05 from footprint level (layer B), and two samples HU-21-02 and HU-21-04 from AU1 (layer C) located at 0.5 m and 1.0 m above the tracks, respectively. Samples were extracted by hammering opaque PVC tubes horizontally at each level and processed in the Luminescence Dating Laboratory of the National Research Centre on Human Evolution (CENIEH) at Burgos, Spain. Quartz grains on the size interval 180–250 μm were extracted from each sample by density in the 2.62–2.7 g cm-3 fraction, under controlled light conditions using standard procedures (Wintle, 1997). Subsequently, they were treated with HCl to eliminate carbonates, H_2O_2 to remove organic matter, and HF 40% during 45 min to dissolve possible remains of feldspar and etch the outer layer of the quartz grains.

Luminescence measurements were carried out in an automated Risø OSL/TL reader (TL-DA 20) with a calibrated $^{90}Sr/^{90}Y$ beta source delivering ~0.10 Gy/s at the sample disc location. Multigrain measurements were stimulated with a blue (470 nm) LED array and single grains were stimulated with a green (532 nm) laser. Derived OSL signals were detected through a U-340 filter. These were measured using a SAR protocol (Murray and Wintle, 2000) with a preheat temperature of 200 °C, assigned according to a preheat dose recovery test carried out on artificially bleached and irradiated aliquots. Individual doses derived from the OSL used for the burial dose estimation were measured on small (1 mm) multi-grain aliquots. In addition, test have been carried out on larger (3 mm) multi-grain aliquots and single grains.

Environmental dose rates were calculated from the contribution of beta, gamma and cosmic radiation. Beta and gamma were based on the radionuclide concentration in the bulk material of the sample matrix measured with ICP-MS, summarized in Table 1. A linear accumulation of sediments has been assumed in order to calculate the contribution of cosmic radiation according to varying burial depth (Prescott and Hutton, 1994). A water content of 20 ± 5% has been considered representative of the burial period. Attenuation caused by moisture and grain size (Bell, 1979; Guerin et al., 2012) was taken into account. The total dose rates were calculated using the Dose Rate and Age Calculator (DRAC, Durcan et al., 2015) and are summarized in Table 2.

Table 1
Radionuclide concentration derived from ICP-MS measurements and sample depth used to calculate the contribution of the cosmic radiation.

Sample	Depth (m)	^{40}K (%)	^{232}Th (ppm)	^{238}U (ppm)	Rb (ppm)
HU-21-04	11	1,06 ± 0,04	3,77 ± 0,13	0,80 ± 0,03	54,8 ± 1,8
HU-21-02	12	1,08 ± 0,04	3,60 ± 0,12	0,83 ± 0,03	53,1 ± 1,8
HU-21-05	12	0,92 ± 0,04	2,52 ± 0,09	0,51 ± 0,02	39,5 ± 1,3
HU-20-01	12	1,02 ± 0,04	1,75 ± 0,06	0,50 ± 0,02	41,4 ± 1,4

2.2. Observations on the burial doses

OSL measurement on multi-grain aliquots of 1 mm (<20 grains per aliquot) and 3 mm (~100 grains per aliquot) provide different dose distributions. While those derived from 1 mm show a main peak centred around the lowest doses, the 3 mm are centred around much higher doses (Fig. 2). The measurement of smaller aliquots makes it possible to obtain higher resolution in dose, allowing to detect the low doses as well as the higher ones. In order to increase the dose resolution even more, single grains (SG) were also measured. The SG distributions are largely scattered with values ranging from 50 to 500 Gy for all four samples, leading to overdispersion values above 50% (Fig. 3). Such a mixture in the doses could be due to the presence of grains with different degree of bleaching (i.e. exposure to sunlight during transport to reset the luminescence signal before being buried) which could lead in some grains carrying a residual dose that was not reset during transport. It has also been pointed out that the distributions from single grains might present a large scatter due to heterogeneity in the dose rate (i.e. different grains would have received different doses during their burial period, Guerin et al., 2015). In the present study, the dose distributions derived from SG show a cluster at the lower doses and then a smaller number of higher dose values (this can be observed clearly in the SG distribution of sample HU21-02 in Fig. 3). The dose rate heterogeneity would cause a large scatter but not a skewness towards higher dose values like that observed. The shape of the SG distributions suggests that the source of the variability in the doses is due to the different degrees of bleaching rather than the dose rate heterogeneity. Nevertheless, to avoid the scatter cause by potential environmental dose rate heterogeneity and variations in the internal potassium content, both difficult to quantify, we have avoided the use of SG for estimating the burial dose.

The hypothesis of incomplete bleaching affecting these sediments is supported also by the 3 mm aliquots, providing an average signal of many grains, showing much higher dose values (Fig. 2). From the SG measurements, 30% of the grains giving light had natural doses above the saturation of the dose response curve, showing again that a large number of grains carry residual doses.

Table 2
Summary of OSL dating results including the environmental dose rates, estimated burial doses and the derived ages reported at 1sigma. The sample code assigned at the luminescence dating laboratory of the CENIEH has been included.

Sample	Lab code	Dose rate (Gy/ka)	Burial dose (Gy)	Age (ka)
HU-21-04	**LM21170-01**	1,27 ± 0,05	155,1 ± 8,6	122 ± 8
HU-21-02	**LM21170-02**	1,27 ± 0,05	168,7 ± 10,5	132 ± 10
HU-21-05	**LM21170-03**	1,03 ± 0,05	154,8 ± 9,1	151 ± 11
HU-20-01	**LM21170-04**	1,06 ± 0,05	159,1 ± 9,5	150 ± 11

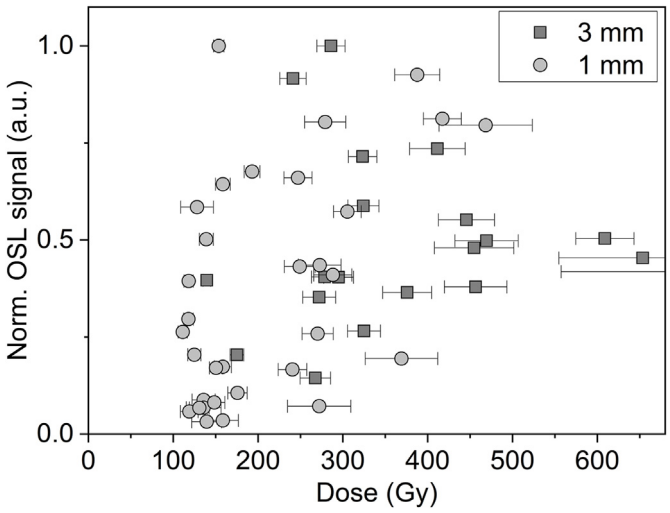

Fig. 2. Dose distribution of sample HU21-05 derived from the measurement of 1 mm aliquots containing <20 grains each, and 3 mm containing around 100 grains each. The one derived from the smaller aliquots is more scattered but provides a better resolution in doses showing individual values in the low dose region as well as larger dose values. The distribution derived from the larger aliquots is centred around a much higher doses than that from small aliquots. The individual doses derived from the 3 mm aliquots are the result of the averaging effect of signal from grains with low equivalent doses and those carrying a residual dose as a result of incomplete bleaching.

Only sample HU21-02, corresponding to a paleosol, show only a 20% of them above saturation. This is contrary to what would be expected as Aeolian sediments do not often present a problem in terms of their optical ressetting (Duller, 2004). Nevertheless, incomplete bleaching of Aeolian sediment has been reported in other studies (Kalińska et al., 2023).

Due to not being able to get a dose values for the grains with a signal above saturation, the SG dose distributions would therefore be missing a significant component in the high dose region (>500 Gy). In contrast, only 10% of the measured multi-grain aliquots are beyond the saturation of the dose response curve and thus, it would not cause a bias in the distribution.

Small multi-grain aliquots (1 mm) have been preferred to obtain representative dose distributions (Fig. 3) as they avoid the averaging effect of larger multi-grain aliquots, provide as high resolution on doses as single grains, but the sources of variability that affect the latter are less pronounced.

2.3. Determination of the burial dose

Since the 1 mm-derived population includes large doses corresponding to incompletely bleached grains, these should be identified and excluded from the calculation, in order to estimate the true burial dose. For that purpose, the internal-external unity approach (IEU, Thomsen et al., 2007) has been considered

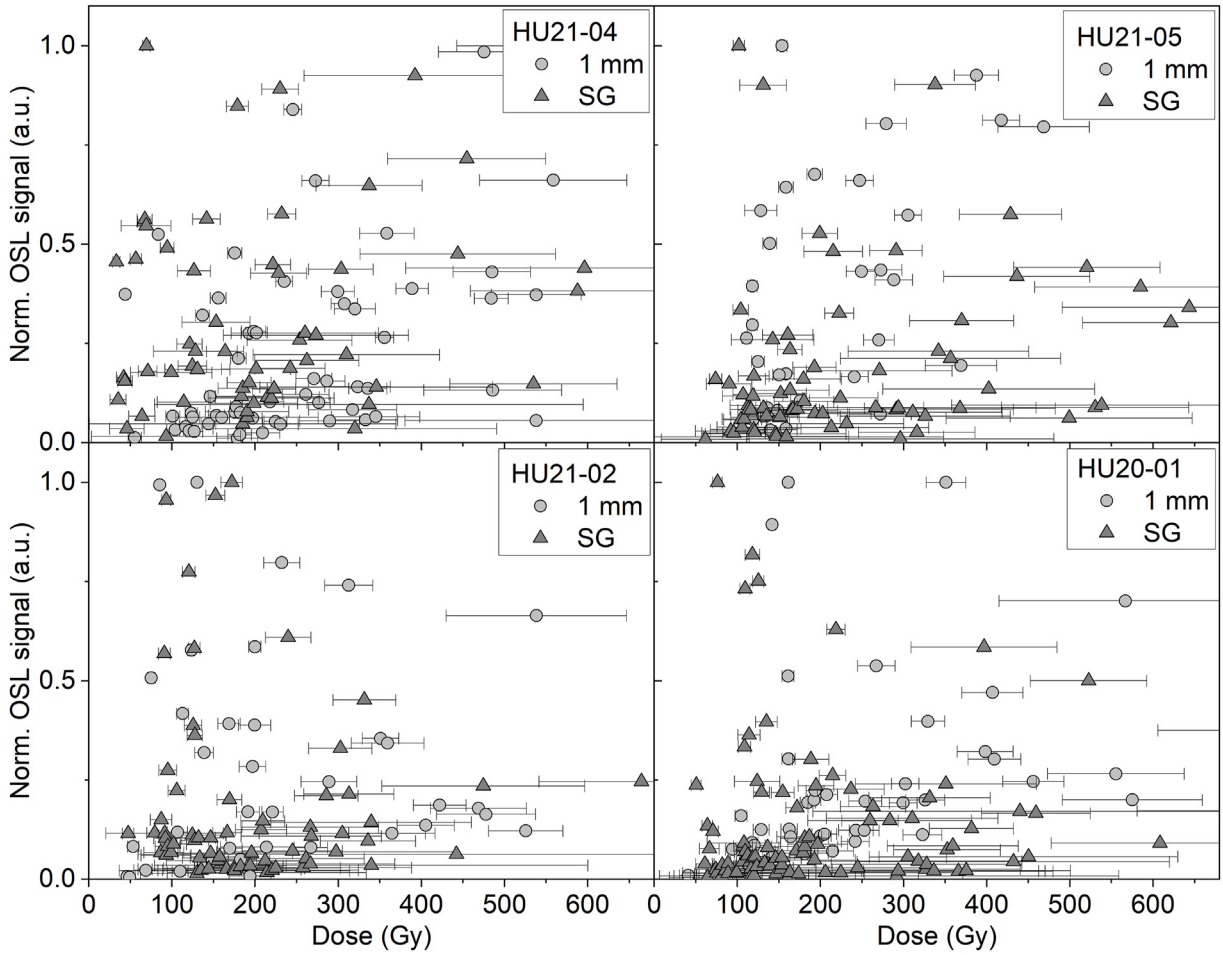

Fig. 3. Dose distributions derived from the OSL measurement of small (1 mm) multi-grain aliquots (circles) and single grains (triangles) of four samples.

appropriate. The IEU approach estimates a burial dose based lowest normal-dose population; presumed to be the population most likely to belong to well-bleached grains. In order to identify the well-bleached population, dose recovery experiments were performed. For these experiments, grains were artificially bleached and irradiated with a known dose in the laboratory. This process eliminates the effect of extrinsic factors, like incomplete bleaching, and makes it possible to obtain a dose distribution only affected by intrinsic factors. In addition, these tests also provide robustness to the method by confirming that a given dose can be recovered with the measurement procedure applied. The dose recovery experiments have been carried out on sample HU20-01 (given doses at 0, 100, 200 and 320 Gy; n = 6), sample HU21-05 (given dose at 300 Gy; n = 6) and HU21-02 (given doses at 0, 100, 200 and 310 Gy; n = 4). The overdispersion for each sample were 10%, 6% and 27% respectively. The less restrictive results, i.e. those from HU21-02, have been used to determine the parameters for the IEU approach (Fig. 4). Derived ages are summarized on Table 2.

2.4. Discusion on the OSL results

The extensive set of measurements carried out on these four samples, including 3 different aliquot sizes and involving a total of 400 multi-grain aliquots and 2400 single grains provides, both, the necessary information for robustly date this site but also, additional information to understand the behaviour observed in the OSL signal.

The large differences between the natural dose distributions and those derived from the dose recovery experiments shows the impact of extrinsic factors on the natural dose populations. The shape of the single grain natural distributions, skewed towards higher doses than the dominant cluster suggest that the main extrinsic factor affecting these sediments is the incomplete bleaching of grains. Therefore, a minimum age approach has been considered necessary to estimate the true burial dose and derived ages summarized in Table 2. Nevertheless, ages were also estimated using the Central Age Model (CAM, Galbraith et al., 1999) to provide a comparison with the IEU ages. Despite identifying an averaging effect leading to high doses when measuring large (3 mm) multi-grain aliquots, CAM was also applied on the 3 mm-derived dose population to allow comparison with ages published by other authors (Mayoral et al., 2022). Note that in this study, 3 mm aliquots were not measured for sample HU20-01 and therefore, the corresponding age is not provided. In all cases CAM was applied on the reduced dose distribution, excluding the outliers identified as those values outside 1.5 times the interquartile range (Tukey, 1977). Ages derived from the CAM on the 1 mm population are slightly older than the IEU ones but no major differences are observed (Table 3). This was anticipated since the outliers excluded remove a large number of the high dose values. These ages are not comparable with those reported by Mayoral et al. (2022) (Fig. 1) and it is only the 3 mm-derived burial doses that lead to similar results to their study. This comparison points out the importance of having high resolution in doses to make it possible to draw a representative dose distribution.

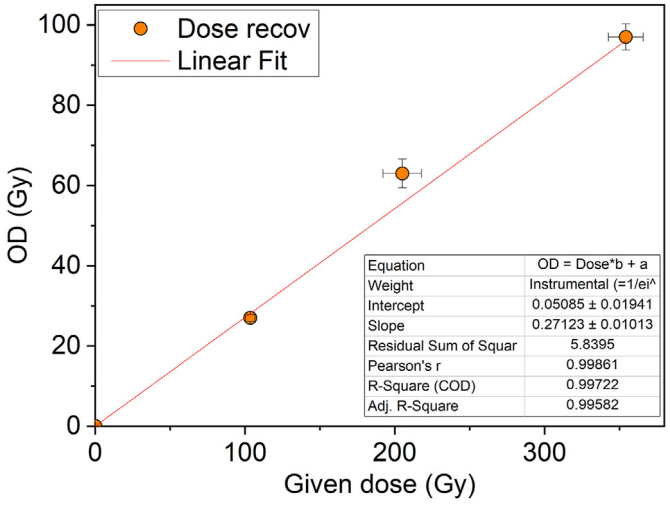

Fig. 4. Figure S2. Linear fit of the given doses at a dose recovery test of sample 21170-03 and corresponding overdispersion of the derived distributions. The slope and intercept provide the parameters for the IEU approach.

3. *In situ* lithic industry

The association of Pleistocene hominin footprints and lithic industries is only known in a few cases worldwide (Altamura et al., 2018), and can be helpful in determining the specific hominin responsible for the footprints. This is the case of the MTS, where the lithics were found at the same stratigraphic level and in close spatial relationship with the hominin footprints (Fig. 5A and B). The lithics found *in situ* were located with GPS by our field intervention team (coordinated by the archaeologist J.M. García) every since J.M. Galán detected the presence of industries and everytime there has been partial exposures of the MTS due to storms, and mapped together with the tracks (Fig. 5A). It has been possible to identify a homogeneous collection composed of 126 lithics (Fig. 5C and D).

In relation to the knapping strategies and operational chains, the lithics (Fig. 6) were divided into four typological groups: (a) flakes without retouching; (b) cores; (c) tools; and (d) splinters. We also noted the representation of the different raw materials and their probable provenance. Within the set of lithics recovered in the MTS, the majority present a fresh and homogeneous appearance, with only occasional and light patinas. In reference to the typologies, there are 15 flakes without retouching, internal and the semi-cortical ones being well represented. Quartzite accounts for 80% of these and quartz (13.3%) and rhyolite (6.6%) being also represented. The identified 15 cores, correspond to centripetals and unipolars mostly made of quartzite (40%) and quartz (46.6%), with the rare presence of other materials such as volcanic rocks, rhyolite and dacite (6.2%). With regard to splinters and chips, they account for 57.7% of the total industry recovered where quartz is mainly represented (62.7%), and lesser by quartzite (27.9%), and volcanic rocks such as rhyolite (6.9%) and dacite (2.35%). Finally, and in relation to the retouched tools, the presence of these is very scarce, two quartzite sidescrapers with simple retouching, one of them of the thorn type, one sidescraper on flint, and one flake with the presence of a notch on quartzite. It is worth to mention the presence of 6 tools, as well as a single Levallois-type core and 4 Levallois splinters (Fig. 6). The typometric study of both the flakes and the negative flake scars point to a production mainly of small and medium-sized flakes, ranging between 2 and 3 cm.

The provenance of raw materials for the lithics must be related with the fluvial terraces of the Guadalquivir River (made of clasts including quartzites and the other lithologies), which can be found less than 10 km away from the MTS. This river drains the Iberian Pyrite Belt where hydrothermal quartz and volcanosedimentary successions are cropping out 50–60 km away from the MTS.

We find parallels to the MTS lithic assemblage, in terms of the technological features that fit within the Mousterian together with systems of direct use with the presence of worked pebbles, in lithic assemblages very close in space, in the same province of Huelva, and in estuarine environments such as those of Terrazas del Odiel I

Table 3
Estimated burial doses and corresponding ages derived from the OSL signal of 1 mm and 3 multi-grain aliquots. The burial dose was estimated applying CAM on the reduced (excluding outliers) populations.

Sample	Lab code	1 mm aliquots (<20 grains)		3 mm aliquots (~100 grains)	
		Burial dose (Gy)	Age (ka)	Burial dose (Gy)	Age (ka)
HU-21-04	**LM21170-1**	192,8 ± 12,8	152 ± 12	324,5 ± 20,9	256 ± 20
HU-21-05	**LM21170-2**	177,7 ± 10,7	140 ± 10	308,9 ± 24,6	243 ± 22
HU-21-02	**LM21170-3**	181,0 ± 18,9	177 ± 20	288,5 ± 34,5	281 ± 36
HU-20-01	**LM21170-4**	188,4 ± 16,2	178 ± 17		

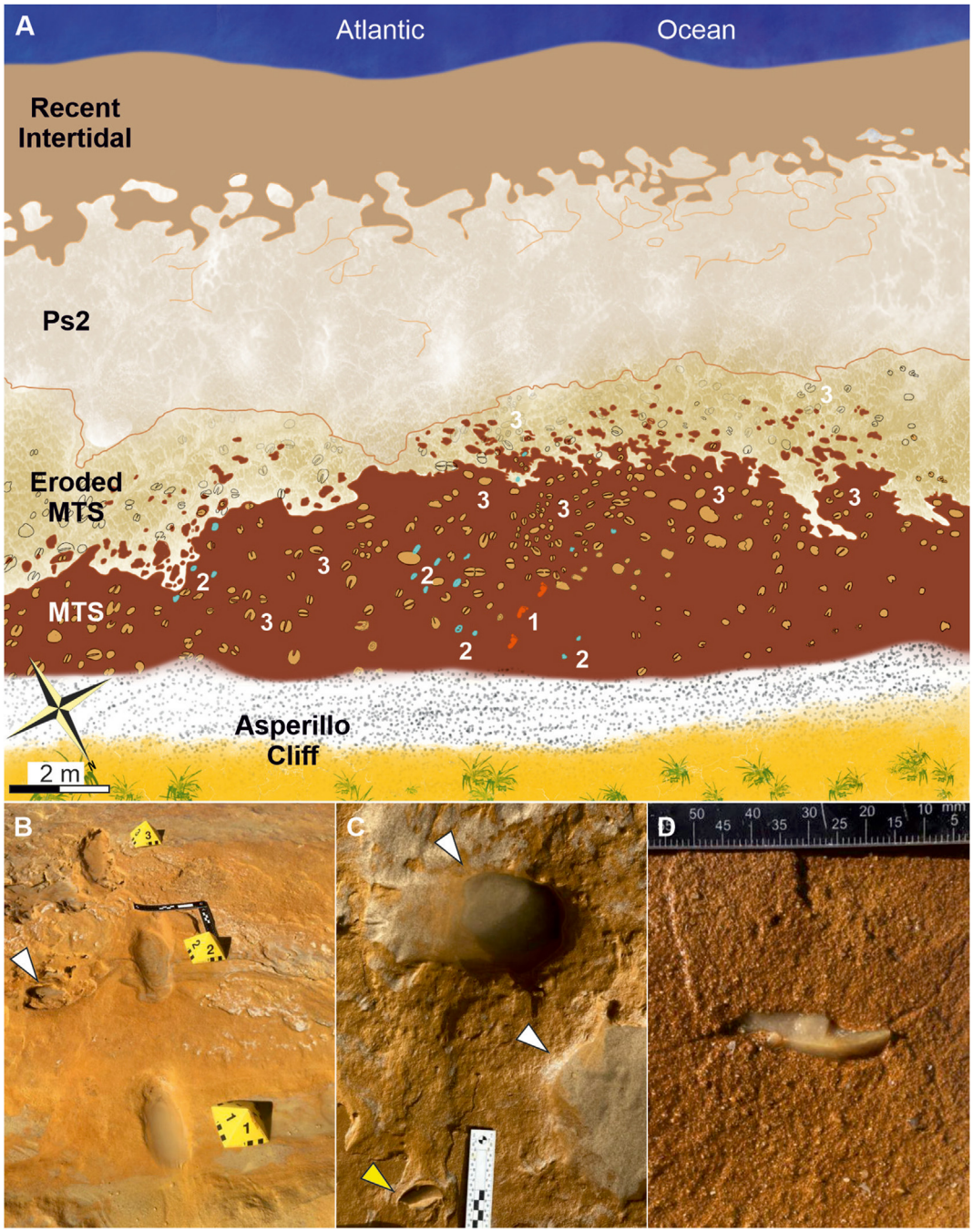

Fig. 5. (A) Map with the location and exact relations between the Neanderthal trackway in Fig. 5B (1), distribution of Mousterian-type industry (2) and potential prey tracks (3) in the MTS. (B) Hominin trackway attributed to a neanderthal adult male and well-preserved cervid track (white triangle) in an exposed area of the MTS. (C) Relation to the bovidae footprints (white triangles) and quartzite artifact (yellow triangle). (D) quartzite artifact embedded into MTS.


1
2
3
4
5
6
7
8
9
10
11
12
1
4 cm

and II in Aljaraque (Campos Jara, 2018), or those of Grillito and Camino de la Coronilla also on the terraces of the same river, or in the Gravera del Apeadero on the terraces of Tinto in Niebla (Vallespí Pérez et al., 1986). El Aculadero site at the coast of Cádiz (Querol and Santonja, 1983) is characterized by a high number of pebbles worked together with Levallois and discoid techniques on quartzite cobbles from local deposits, being dated by OSL between 110–63 ka BP (Santonja and Pérez González, 2010). In the Guadalquivir basin, the Tarazona III site stands out, with OSL dates between 138 ka and <110–104 ka BP (Caro et al., 2011), with the presence of worked pebbles and the exploitation of small-sizes flakes (Caro Gómez et al., 2021). Small-sized flakes and with the presence of quartz as raw material is also documented in the Cova del Rinoceront (Daura et al., 2015), in the province of Barcelona, presenting chronologies between 147 and 74 ka. Already with later chronologies, in level IV of the Gorham's Cave (Gibraltar), the exploitation of small lithics is documented, with a predominance of discoid strategy on local massive sandstones and the presence of some pebbles worked on limestone (Giles-Pacheco et al., 2012). Between 50–40 ka, in the peninsular area these small-sized lithics are documented in sites such as Axlor, Amalda cave or Quebrada shelter (Ríos-Garaizar et al., 2015). Therefore, the MTS lithic industry shows characteristics, although scarcely documented in earlier stages (Fernández-Peris et al., 2020; Santonja et al., 2005), that fit within the Mousterian technological variabilities widespread in the Iberian Peninsula during the MIS 6/5 until MIS 3.

4. Discussion and implications

The Asperillo Cliff succession has been widely studied since the 1960s from the sedimentological and pedological, geomorphological, tectonic and palaeobotanical perspectives (Rodríguez-Ramírez, 1998; Zazo et al., 2005; Roquero et al., 2013; Fernández et al., 2021, and references therein). The result of this work has been the modeling and characterizing of the complex evolution of this entire sector, controlled by the interaction of littoral processes and sea-level changes in an emerging coastal plain (Zazo et al., 2005). This is the generally accepted model (see Fig. 1B) for the evolution of the site (e.g., Rodríguez Vidal et al., 2014 and references therein).

Along the cliff, Zazo et al. (2005) and Rodríguez-Vidal et al. (2014) distinguished in ascending stratigraphic order (Fig. 1B), palaeosols (Ps1 of pre-MIS 5 age and Ps2 attributed to this period), fluvial deposits (coastal swampy flood plain), beach deposits (shoreface to foreshore facies dated from MIS 5), and aeolian deposits (seven wind units from AU1 to AU7), ranging from late MIS 5 to early MIS 4 (AU1), MIS 4-2 (AU2), late Pleistocene-early Holocene (AU3) and the last 5000 years (AU4 to AU7). An important gravitational fault (Torre del Loro Fault - TLF) has been identified, dividing the cliff into two different sectors (Fig. 1B): the upthrown fault block (UFB), located to the NNW, with outcrops of fluvial and marine depositional facies at the base; and the downthrown fault block (DFB), located to the SSE and of which the Matalascañas sector would form part, with a predominance of aeolian facies.

The geochronological framing of this model has been based on a number of dates obtained. These dates have been obtained via radiocarbon (e.g., Zazo et al., 1981, 2008; Fernández et al., 2021), archaeological (i.e., lithic industries, Borja and Díaz del Olmo, 1992; Borja et al., 1999) and also Optically Stimulated Luminescence (OSL). Regarding the latter, it is worth highlighting that the compilation of OSL ages from Zazo et al. (2005) carried out in the two blocks differentiated by the TLF, with five samples analyzed in each UFB and DFB blocks (Fig. 1B), generated dates of up to 106 ± 19 ka (1sigma level), and not older. Thus, in the DFB, five dates were carried out: two of them near at the base of the cliff, in the same sector of Matalascañas where the footprints later appeared (Neto de Carvalho et al., 2020) and the remaining three in a sector further to the W, closer to TLF (Fig. 1B). The oldest sample corresponds to AU1, located above the paleosol Ps2, with an OSL age of 106 ± 19 ka. The second dated sample would be located in AU2, a little less than 2 m above the previous one, with an age of 74 ± 7 ka. The remaining three, further to the W, correspond to higher sections of AU2 (48 ± 5 and 32 ± 3 ka) and AU3 (16 ± 3 ka).

For their part, Mayoral et al. (2022), in the same area of the Matalascañas DFB, performed new OSL dating of the paleosol Ps2 and the wind units that cover it (Fig. 1C). As for the Ps2, it is true that it had not been previously dated, but it has always been considered in its regional context as belonging to the Middle-Late Pleistocene transition (Zazo et al., 2005; Roquero et al., 2013), making the difference with the units dated by Mayoral et al. (2022) much more striking (compare Fig. 1B and 1C). These differences can hardly be attributed to improvement in OSL analysis or to different laboratorial standards.

The new dates of Mayoral et al. (2022) do not fit in the previous chronostratigraphic model, despite this also includes dated samples in the UFB (Zazo et al., 2005) with the same methodology and with results consistent with those obtained at the Matalascañas site (see Fig. 1C). Our OSL dates obtained for Ps2 and AU1 presented in Table 2 match well with the previous results of Zazo et al. (2005) (compare Fig. 1B and 1D), being less than half the age obtained by Mayoral et al. (2022) using the same geochronological method (compare Fig. 1C and 1D). These two sets of disparate ages have implications regarding the origin of the tracks and lithic industry found in the MTS. The 87 recently described hominin footprints from the MTS (Mayoral et al., 2021), suggesting a multi-aged social group dominated by non-adults exploiting, at least temporarily, the coastal resources were attributed to *Homo heidelbergensis* (or pre-Neanderthals) according to Mayoral et al. (2022). Their ages, based on the OSL signal of large multi-grain aliquots, suffer from the averaging effect derived from the measurement of many grains together. In a well-bleached (i.e. sufficiently exposed to sunlight prior to deposition) this averaging effect would not have had any implications. In the samples studied here, measurement of smaller aliquots and single grains have made it possible to increase the resolution on doses. The derived distributions show a population of grains with different degrees of bleaching. Only by excluding the dose values most-likely to be affected by incomplete bleaching, the true burial dose can be estimated. Their results, solely based on the OSL ages are not backed by lithic evidence (following the model of Shea, 2013). If our OSL ages matching the ones of Zazo et al. (2005) are correct, it becomes clear that the most parsimonious allocation of the hominin footprints has to be to the Neanderthals.

Thus, the MTS represents an extraordinary case where Neanderthal footprints are temporal (no more than hours or a day) and spatially close associated to other tracks and trackways of large herbivores (Neto de Carvalho et al., 2020a; b, 2021, 2022) and archaeological evidence (lithic industry, Mode 3 with presence of Mode 1 of expeditious character). The overstepping of animal tracks together with slow walking gait observed in the Neanderthal trackways (Fig. 5B as example) allow to infer possible stalking behavior (Neto de Carvalho et al., 2021), and the presence of lithic

Fig. 6. Mousterian lithic assemblage retrieved in the MTS: 1. Discoid core in quartzite, 2. Discoid core in quartz, 3–4. Levallois flakes in quartzite, 5. Internal flake in quartzite, 6. Internal flake in dacite, 7. Bipolar flake in quartzite, 8. Flake in quartzite, 9. Side scraper thorn type, 10. Internal flake in quartzite, 11. Semicortical flake in quartzite, 12. Worked pebble in dacite.

tools associated to the MTS is compelling evidence for animal processing. Moreover, the short-range provenance, and expeditious character of the lithic tools, are not evidence for settlement, but rather as a place of passage, both for the fauna and for the Neanderthals.

Author contributions

Carlos Neto de Carvalho: Conceptualization, Writing - Original Draft.; Fernando Muñiz: Conceptualization, Validation, Writing - Original Draft.; Luis M. Cáceres: Funding acquisition, Visualization, Writing - Review & Editing.; Joaquín Rodríguez-Vidal: Project administration, Supervision; Alicia Medialdea: Resources, Methodology, Formal analysis.; Miren del Val: Resources, Methodology, Formal analysis.; Pedro Proença Cunha: Validation, Funding acquisition.; José María García: Resources, Investigation.; Francisco Giles-Guzmán: Investigation, Visualitation; José S. Carrión: Conceptualization.; Zain Belaústegui: Validation.; Antonio Toscano: Resources, Investigation.; Paula Gómez: Resources, Investigation.; José María Galán: Resources.; João Belo: Validation.; Mario Cachão: Validation.; Francisco Ruiz: Funding acquisition.; Samuel Ramirez-Cruzado: Resources.; Geraldine Finlayson: Resources.; Stewart Finlayson: Resources.; Clive Finlayson: Supervision.

Declaration of competing interest

The authors declare that they have no known competing financial interests or personal relationships that could have appeared to influence the work reported in this paper.

Data availability

Data will be made available on request.

Acknowledgments

Research was possible thanks to the Delegaciones territoriales de Huelva, Consejería de Agricultura, Ganadería, Pesca y Desarrollo Sostenible and Consejería de Cultura (Junta de Andalucía), Servicio de Geodiversidad y Biodiversidad (Dirección General de Medio Natural, Biodiversidad y Espacios Protegidos) and The National Park of Doñana. This work has been supported by the Research Groups RNM-293 and RNM-238, University of Huelva & Junta de Andalucía. This work also received institutional support from the Naturtejo, E.I.M. (Naturtejo UNESCO Global Geopark). We would like to thank to Dr. Teodosio Donaire (Department of Earth Sciences, University of Huelva) by the petrological classification of the lithic industry. This work was partly funded by the Fundação para a Ciência e Tecnologia, through: (i) projects UIDB/04292/2020 & UIDP/04292/2020 (MARE - Marine and Environmental Sciences Centre) and LA/P/0069/2020 (ARNET). Funding for open access charge: Universidad de Huelva / CBUA.

References

Altamura, F., Bennett, M.R., D'Août, K., et al., 2018. Archaeology and ichnology at Gombore II-2, Melka Kunture, Ethiopia: everyday life of a mixed-age hominin group 700,000 years ago. Sci. Rep. 8, 2815.

Bell, W.T., 1979. Attenuation factors for the absorbed radiation dose in quartz inclusions for thermoluminescence dating. Ancient TL 8, 1–12.

Borja, F., Díaz del Olmo, F., 1992. Eastern sector of the cliffs at El Asperillo (Huelva coast, SW Spain): formation and chronology. MBSS Newsletter 14, 87–93.

Borja, F., Zazo, C., Dabrio, C.J., et al., 1999. Holocene aeolian phases and human settlements along the Atlantic coast of southern Spain. Holocene 9, 333–339.

Campos Jara, P., 2018. El Paleolítico de Río Odiel I (Aljaraque, Huelva) contribución al estudio de su definición estratigráfica. In: Campos Jara, P. (Ed.), Arqueología y territorio en la provincia de Huelva: veinte años de las Jornadas de Aljaraque (1998-2017), pp. 19–67.

Caro, J.A., Díaz del Olmo, F., Cámara, R., Recio, J.M., y Borja, C., 2011. Geoarchaeological alluvial terrace system in Tarazona: chronostratigraphical transition of mode 2 to mode 3 during the Middle-Upper Pleistocene in the Guadalquivir River valley (Seville, Spain). Quat. Int. 243, 143–160.

Caro Gómez, J.A., Díaz del Olmo, F., Barba Herrero, L., et al., 2021. Paleolítico Medio del Guadalquivir: las industrias de pequeñas lascas del yacimiento Tarazona III (Sevilla, España). Spal 30 (1), 9–45.

Daura, J.M., Sanz, R., Julià, D., et al., 2015. Cova del Rinoceront (Castelldefels, Barcelona): a terrestrial record for the Last Interglacial Period (MIS 5) in the Mediterranean Coast of the Iberian Peninsula. Quat. Sci. Rev. 114, 203–227.

Duller, G.A.T., 2004. Luminescence dating of Quaternary sediments: recent advances. J. Quat. Sci. 19, 183–192.

Durcan, J.A., King, G.E., Duller, G.A., 2015. DRAC: dose rate and age calculator for trapped charge dating. Quat. Geochronol. 28, 54–61.

Fernández, S., Carrión, J.S., Ochando, J., et al., 2021. New palynological data from the late Pleistocene glacial refugium of South-west iberia: the case of Doñana. Rev. Palaeobot. Palynol. 290, 104431.

Fernández-Peris, J., Cuartero, F., Barciela, V., et al., 2020. The flake microlithism in the European Pleistocene: the case of Bolomor cave (MIS 9-5, Valencia, Spain). J. Archaeol. Sci.: Report.

Galbraith, R.F., Roberts, R.G., Laslett, G.M., Yoshida, H., Olley, J.M., 1999. Optical dating of single and multiple grains of quartz from Jinmium rock shelter, northern Australia: Part I, experimental design and statistical models. Archaeometry 41, 339–364.

Giles Pacheco, F., Giles Guzmán, F.J., Gutiérrez López, J.M., et al., 2012. The tools of the last Neanderthals: morphotechnical characterisation of the lithic industry at level IV of Gorham's Cave, Gibraltar. Quat. Int. 247, 151–161.

Guerin, G., Mercier, N., Nathan, R., Adamiec, G., Lefrais, Y., 2012. On the use of the infinite matrix assumption and associated concepts: a critical review. Radiat. Meas. 47, 778–785.

Guerin, G., Jain, M., Thomsen, K., Murray, A., Mercier, N., 2015. Modelling dose rate to single grains of quartz in well-sorted sand samples: the dispersion arising from the presence of potassium feldspars and implications for single grain OSL dating. Quat. Geochronol. 27, 52–65.

Kalińska, E., Weckwerth, P., Alexanderson, H., 2023. Recent advances in luminescence dating of the late quaternary sediments in the Baltic States, northern europe: a review. Earth Sci. Rev. 236, 104272.

Mayoral, E., Díaz-Martínez, I., Duveau, J., Santos, A., Ródríguez-Ramírez, A., Morales, J.A., Morales, L.A., Díaz-delgado, R., 2021. Tracking late Pleistocene Neandertals on the Iberian coast. Sci. Rep. 11, 4103.

Mayoral, E., Duveau, J., Santos, A., Ródríguez-Ramírez, A., Morales, J.A., Rivera-Silva, J., Gómez-Olivencia, A., Díaz-Martínez, I., 2022. New dating of the Matalascañas footprints provides new evidence of the Middle Pleistocene (MIS 9 8) hominin paleoecology in southern Europe. Sci. Rep. 12, 17505.

Murray, A.S., Wintle, A.G., 2000. Luminescence dating of quartz using an improved single-aliquot regenerative-dose protocol. Radiat. Meas. 32, 57–73.

Neto de Carvalho, C., Muñiz, F., Galán, J.M., et al., 2020a. First vertebrate tracks and palaeoenvironment in a MIS-5 context in the Doñana National Park (Huelva, SW Spain). Quat. Sci. Rev. 243.

Neto de Carvalho, C., Muñiz, F., Belaústegui, Z., et al., 2020b. Paleoecological implications of large-sized wild boar tracks recorded during the Last Interglacial (MIS 5) at Huelva (SW Spain). Palaios 35 (12).

Neto de Carvalho, C., Belaústegui, Z., Toscano, A., et al., 2021. First tracks of newborn straight-tusked elephants (*Palaeoloxodon antiquus*). Sci. Rep. 11, 17311.

Neto de Carvalho, C., Muñiz, F., Cáceres, L.M., et al., 2022. Aurochs roamed along the SW coast of Andalusia (Spain) during late Pleistocene. Sci. Rep. 12, 9911.

Prescott, J.R., Hutton, J.T., 1994. Cosmic ray contributions to dose rates for luminescence and ESR: large depths and long-term time variations. Radiat. Meas. 23, 497–500.

Querol, M.A., Santonja, M., 1983. El yacimiento de cantos trabajados de El Aculadero (Puerto de Santa María, Cádiz), vol. 130. Excavaciones Arqueológicas en España, Madrid.

Ríos-Garaizar, J., Eixea, A., Villaverde, V., 2015. Ramification of lithic production and the search of small tools in Iberian Peninsula Middle Paleolithic. Quat. Int. 361, 188–199. https://doi.org/10.1016/j.quaint.2014.07.025.

Rodríguez-Ramírez, A., 1998. Geomorfología del Parque Nacional de Doñana y su entorno. Organismo Autónomo Parques Nacionales.

Rodríguez-Vidal, J., Bardají, T., Zazo, C., et al., 2014. Coastal dunes and marshes in Doñana National Park. In: Gutiérrez, F., Gutiérrez, M. (Eds.), Landscape and Landforms of Spain. Springer Science+Business Media, pp. 229–238.

Roquero, E., Silva, P.G., Zazo, C., et al., 2013. Micromorphology of hydromorphic soils developed in fluvio-marine sediments during the middle-late Pleistocene transit in the Gulf of Cadiz (Atlantic South Spain). Spanish Journal of Soil Science 3 (3), 184–200.

Santonja, M., Panera, J., Rubio-Jara, S., Pérez-González, A., 2005. La industria lítica de Ambrona. Características generales y contexto estratigráfico. In: Santonja, M., Pérez-González, A. (Eds.), Los yacimientos paleolíticos de Ambrona y Torralba (Soria). Un siglo de investigaciones arqueológicas, vol. 5. Zona Arqueológica, pp. 306–332.

Santonja, M., Pérez González, A., 2010. Precisiones en torno a la edad y la industria lítica de El Aculadero (Puerto de Santa María, Cádiz). Cuaternario y arqueología: homenaje a Francisco Giles Pacheco 18–26.

Shea, J.J., 2013. Lithic modes A–I: a new framework for describing global-Scale variation in Stone tool Technology illustrated with evidence from the east mediterranean levant. J. Archaeol. Method Theor 20, 151–186.

Thomsen, K.J., Murray, A.S., Bøtter-Jensen, L., Kinahan, J., 2007. Determination of burial dose in incompletely bleached fluvial samples using single grains of quartz. Radiat. Meas. 42 (3), 370–379.
Tukey, J.W., 1977. Exploratory Data Analysis. Pearson, London, UK vol. 2.
Vallespí Pérez, E., Álvarez, G., Pérez Sindreu, F. de P., Rufete Tomico, P., 1986. Nuevas atribuciones onubenses al paleolítico inferior y medio. Huelva en su historia 1, 43–56.
Wintle, A.G., 1997. Luminescence dating: laboratory procedures and protocols. Radiat. Meas. 27, 769–817.
Zazo, C., Dabrio, C.J., Goy, J.L., Menanteau, L., 1981. Parada "Torre del Loro"- Guías de excursiones "Estero de Domingo Rubio. Torre del Loro, El Aculadero. Faro de Chipiona". In: Actas V Reunión Grupo Español de Trabajo del Cuaternario, pp. 357–361. Sevilla.
Zazo, C., Dabrio, C.J., Goy, J.L., et al., 2008. The coastal archives of the last 15 ka in the Atlantic–Mediterranean Spanish linkage area: sea level and climate changes. Quat. Int. 181, 72–87.
Zazo, C., Mercier, N., Silva, P.G., et al., 2005. Landscape evolution and geodynamic controls in the Gulf of Cadiz (Huelva coast, SW Spain) during the late quaternary. Geomorphology 68, 269–290.